Online supplementary information

S1 Experimental details and additional experiments

S1.1 Sample preparation method

The rubber used was Kraton G1730 SEPS triblock copolymer containing 22% polystyrene. The manufacturer's datasheet quotes an ultimate elongation of 880%, a Shore A hardness of 60. Uniaxial elongation tests of dogbone samples gave a modulus of 3.3 MPa. The LLDPE films were commercial films (Mitsui HC-50) marketed for food-packaging applications with a thickness of 50 micron quoted by the manufacturer.

The LLDPE films retain some residual stress from the manufacturing process. This was first relieved by heating the films to 90℃, upon which they shrank roughly 10% along one direction. Trilayers were prepared by compression molding the SEPS rubber pellets between sheets of the LLDPE films. The thickness of the rubber was maintained using steel strips as spacers. A platen press (Carver) was used at a temperature of 133℃. The trilayers were then cut into dogbone shapes for tensile testing.

Tensile testing was conducted in a MTS Insight tensile testing machine with a 50N load cell. The nominal test length of the sample (i.e. the distance between the clamps) was ~40 mm, whereas the gauge length of the samples was 20 mm. In the first step, dubbed "stretching", the samples were stretched to the desired strain (50% to 300% based on the nominal test length). Immediately after reaching the desired strain, the samples were allowed to contract at the same rate, a step dubbed "release". The test was stopped when the force recorded reduced to low values and/or the samples bowed visibly.

The testing speed in most of the samples was 100% per minute based on the nominal test length. Limited experiments were conducted at lower (50%/min) and higher (200%/min) speed to verify that test speed did not affect results significantly.

Determining the wrinkle profile requires an edge-on view of the wrinkles, preferably along the length of the dogbone. However, the fact that the face layers are capable of large plastic deformation complicates this situation. First, cutting dogbones may already induce some damage near the edges (even before any stretching), thus, in order to avoid biasing results from edge effects, it is desirable to image the wrinkles near the centerline of the dogbones. Yet, one cannot simply slice along the centerline of the wrinkled samples with a razor: once again, plastic deformation of the face layers induces massive distortion of the wrinkle structure. It is also difficult to cryo-fracture the samples length-wise. Accordingly, the samples were replicated in silicone rubber as described in the main text.

S1.2 Testing for delamination

The geometric mismatch induced in these samples is severe and hence delamination is a potential concern. We tested for delamination directly by examining the samples in SEM as well as in optical microscopy. In occasional cases, some delamination near the edges was evident, but it stopped within 2-3 wavelengths of the edge. The contrast between delaminated and adhered films is very clearly obvious (Fig. S1). Attempts to peel the face layers off from the rubber were unsuccessful. Thus we conclude that delamination does not affect our experiments.

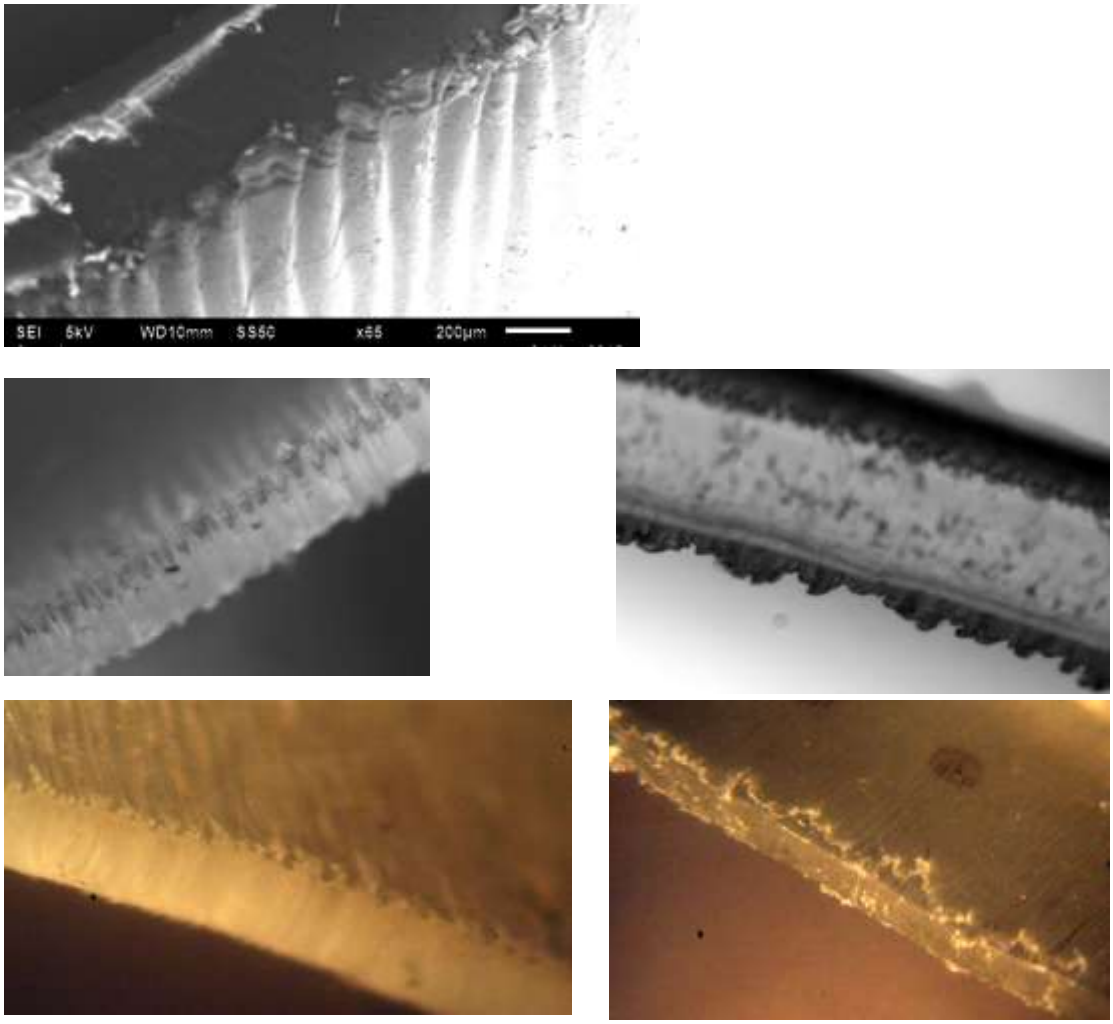

Fig. S1: Left column: SEM (top) and optical (lower) images taken within one day after stretching and releasing the trilayer composite samples showing complete attachment of the plastic film to the rubber. Right column: Optical images of delamination of the film starting from the edge of sample after four days. Note that the delaminated sections remain ruffled indicating plastic deformation in bending.

S1.3 Experiments with other rubber layer thicknesses

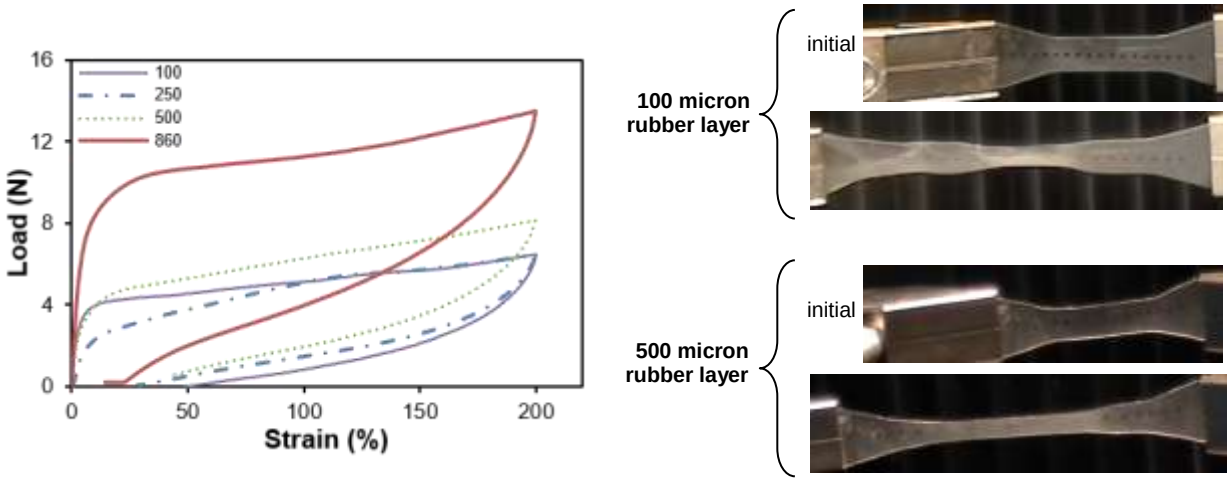

Fig. S2: Stress-strain curves of trilayer samples at various rubber layer thicknesses, H_0, listed in the legend in microns. Curve at 860 microns correspond to the same data as in Fig. 3. The images to the right show the snapshots during stretching of two different trilayer samples. Note that the trilayer with 500 micron thick rubber (left) stretches homogeneously, whereas the one with 100 micron thick rubber (right) shows necking.

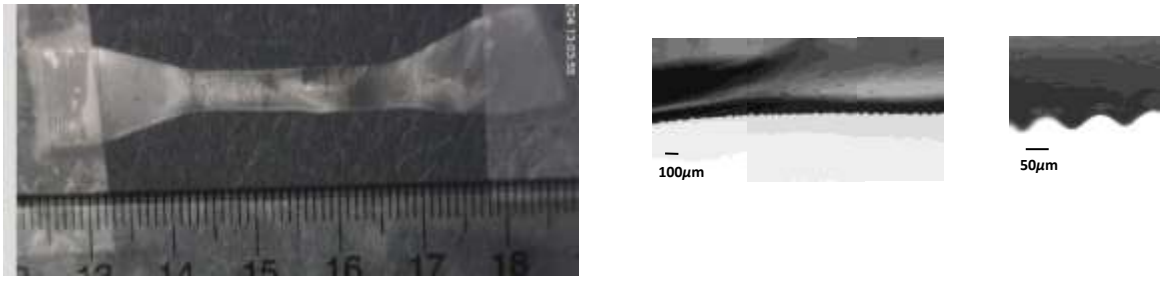

Fig. S3: Image of sample (left) with a 100 micron thick rubber layer with 50 micron face layers after 200% nominal strain. Right: optical images of cross sections of silicone replicas. Even at this small rubber thickness, wrinkles develop with nearly the same wavelength as Fig. 6 in the main text.

S1.4 Experimental tests for necking of trilayers

Two experiments were conducted to test for non-homogeneous thinning of the plastic layer in a trilayer. In the first, samples of the trilayers (with a rubber layer thickness of 860 micron) were stretched in a tension apparatus to a stretch of 2.4. Unlike the equipment used for tensile testing, this apparatus is not capable of measuring loads. However it permits examination of the samples at far higher resolution using a video microscope. This experiment was performed quasi-statically: the sample was slowly stretched to the final length, and allowed to stay stretched for several minutes during video examination. Non-homogeneous deformation was not evident in this experiment. Subsequently, the sample was gradually released with constant video microscopic examination. A key feature of the simulations (Fig. 9 in the main text) is that if necks appear, then during the subsequent release, the buckling is highly non-uniform: the thinned regions buckle first and develop a significant amplitude before the thicker regions buckle. Such localized buckles would almost certainly have been evident in video examination, but instead, we observed only a gradual increase in buckle amplitude everywhere over the sample.

A second experiment was conducted by stretching the samples to a stretch of roughly 2 in a different apparatus. A silicone rubber precursor liquid was poured over this sample while still stretched and allowed to crosslink. The silicone-embedded sample was then then placed in an oven at 70℃ while held stretched. At this temperature, the rubber layer relaxes its tension over several hours (i.e. a free-standing rubber layer recovers very little). Thus upon cooling, when the trilayer sample was extracted from the embedded silicone, it did not change dimensions significantly, i.e. the stretched state was preserved with very little wrinkling. The sample as well as the embedding rubber surfaces were then examined by optical microscopy. Note that this entire procedure is similar to that used for obtaining Fig. 1E, except that the silicone embedding was performed while the sample was held stretched. Both were found to be smooth with no evidence of non-homogeneous thinning. The corresponding silicone replica is shown in Fig. S4. If the film had shown periodic necking behavior, it would likely have induced correspondingly periodic variations in the rubber thickness as well, but this is not evident in Fig. S4.

The fact that these two altogether different experiments did not show evidence of necking suggests that the plastic film thins uniformly.

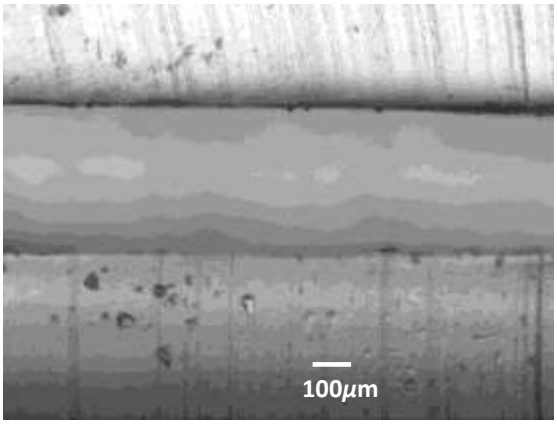

Fig. S4: Image of silicone replica of a sample stretched, embedded in silicone, and then heated. The silicone is an accurate replica of the stretched sample and shows no evidence of periodic variations in thickness.

S2 Simulations

S2.1 Kinematics of deformation

A body Ω_0 in its reference configuration having a material point with position vector $\mathbf{X}$ is considered as shown in Fig. S5. The material point $\mathbf{X}$ is mapped to the point $\boldsymbol{x}$ in the spatial configuration Ω_t by the deformation map φ as $\boldsymbol{x} = \varphi(\mathbf{X}, t)$. The total deformation gradient $\mathbf{F} = \nabla_X \varphi$ is multiplicatively decoupled into two parts as

$$\mathbf{F} = \mathbf{F}_e \mathbf{F}_p \tag{S1}$$

where the elastic distortion of the material is characterized by $\mathbf{F}_e$ while the inelastic deformation is indicated by $\mathbf{F}_p$. The constitutive framework introduces a stress free intermediate state, $\bar{\Omega}_p$. Therefore, the elastic deformation gradient can be written as $\mathbf{F}_e = \mathbf{F}\mathbf{F}_p^{-1}$ (see Fig. S6). The right Cauchy-Green tensor and its elastic counterpart can be given as

$$\mathbf{C} = \mathbf{F}^{\mathrm{T}}\mathbf{F}, \quad \mathbf{C}_e = \mathbf{F}_e^{\mathrm{T}}\mathbf{F}_e = \mathbf{F}_p^{-\mathrm{T}}\mathbf{C}\mathbf{F}_p^{-1} \tag{S2}$$

The total Jacobian, $J = \det(\mathbf{F})$, which also represents the volume change ratio of the material, can be multiplicatively decomposed similar to the deformation gradient as $J = J_e J_p$. Here, $J_e = \det(\mathbf{F}_e) > 0$ and $J_p = \det(\mathbf{F}_p) > 0$. Spatial velocity gradient can be introduced as

$$\boldsymbol{l} = \nabla_x \boldsymbol{v} = \dot{\mathbf{F}}\mathbf{F}^{-1} = \dot{\mathbf{F}}_e\mathbf{F}_e^{-1} + \mathbf{F}_e\dot{\mathbf{F}}_p\mathbf{F}_p^{-1}\mathbf{F}_e^{-1} \tag{S3}$$

with $\boldsymbol{v} = \dot{\boldsymbol{x}}$ denoting the spatial velocity. Pull back of the spatial velocity gradient $\boldsymbol{l}$ to the intermediate configuration yields

$$\mathbf{L} = \mathbf{F}_e^{-1}\boldsymbol{l}\mathbf{F}_e = \underbrace{\mathbf{F}_e^{-1}\dot{\mathbf{F}}_e}_{\mathbf{L}_e} + \underbrace{\dot{\mathbf{F}}_p\mathbf{F}_p^{-1}}_{\mathbf{L}_p'} \tag{S4}$$

which can be additively decomposed into an elastic velocity gradient tensor $\mathbf{L}_e$, and a transformed plastic deformation gradient $\mathbf{L}_p^{\text{¢}}$.

Cauchy stress tensor can be obtained from the strain energy functional Ψ as

$$\boldsymbol{\sigma} = J^{-1}\mathbf{F}\frac{\partial \Psi}{\partial \mathbf{C}}\mathbf{F}^{\mathrm{T}} \tag{S5}$$

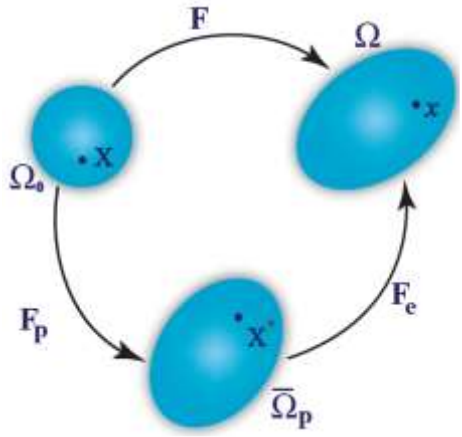

Fig. S5: Graphical representation of multiplicative decomposition of deformation gradient $\mathbf{F}$.

S2.2 Constitutive modeling of the elasto-plastic material

The LLDPE face layer is modeled as a nearly-incompressible (Poisson's ratio 0.45) elastic-perfectly plastic material that is elastic up to the yield point, and subsequently maintains a stress equal to the yield strength without any strain hardening. Accordingly, the constitutive response of the face layer can be captured by two parameters: the modulus prior to yield, E, and the yield strength, σ_y.

The elastic response of LLDPE is modeled by the strain energy function for the nearly-compressible Neo-Hookean material given as

$$\Psi = \frac{\kappa}{2}(J_e - 1)^2 + \frac{\mu}{2}(\bar{I}_1 - 3) \tag{S6}$$

where $k = \frac{E}{3(1-2n)}$ is the bulk modulus and $m = \frac{E}{2(1+n)}$ is the shear modulus. Further, the jacobian is defined as $J = \det(\mathbf{F})$ and $J_e = \det(\mathbf{F}_e)$. Denoting $\mathbf{C} = \mathbf{F}^T\mathbf{F}$ as the right Cauchy–Green tensor, its first invariant is given as $I_1 = \mathrm{tr}\mathbf{C}$, while its deviatoric counterpart is $\bar{I}_1 = J^{-2/3}I_1$.

The inelastic response of the material is characterized by suitably defining (a) yield condition, (b) flow rule and (c) hardening/softening laws. The flow rule of the face layer material is defined in terms of the plastic deformation gradient $\mathbf{L}_p$ as

$$\mathbf{L}_p = \dot{\mathbf{F}}_p\mathbf{F}_p^{-1} = \dot{\gamma}\,\mathbf{N}_p \quad \text{with} \quad \mathbf{N}_p = \frac{\partial g}{\partial \mathbf{M}_e} \tag{S7}$$

where, $\mathbf{N}_p$ describes the direction of the plastic flow, and $\dot{\gamma}$ is the plastic rate parameter. In the above equation, g describes the potential function governing plastic evolution that depends on Mandel stress tensor $\mathbf{M}_e$. In the present formulation, the yield function for the isotropic linearly hardening case

is assumed as the following type

$$f\left(\boldsymbol{M}_e, \bar{\varepsilon}_p\right) = \sqrt{\frac{3}{2}\boldsymbol{M}_e^d : \boldsymbol{M}_e^d} - \left[\sigma_y + H\bar{\varepsilon}_p\right] = 0 \tag{S8}$$

with $\boldsymbol{M}_e^d$ as the deviatoric part of the Mandel stress tensor $\boldsymbol{M}_e$. The yield strength (pushed forward to the intermediate configuration) and hardening modulus are represented as $\boldsymbol{s}_y$ and H, respectively. $\bar{\varepsilon}_p$ is the plastic strain parameter. The hardening parameter is taken as H=0 in this paper.

S2.3 Constitutive modeling of the elastic rubber

The SEPS rubber is modeled as a 2-parameter Mooney-Rivlin material with a strain energy function given by

$$\Upsilon(\bar{I}_1, \bar{I}_2, J) = C_1(\bar{I}_1 - 3) + C_2(\bar{I}_2 - 3) \tag{S9}$$

where C_1 and C_2 are material parameters. $\bar{I}_2$ is the second invariant of the right Cauchy–Green tensor defined as $\bar{I}_2 = J^{-4/3} I_2$. The corresponding engineering stress upon uniaxial elongation is given by

$$\sigma = 2C_1\left(S - \frac{1}{S^2}\right) + 2C_2\left(1 - \frac{1}{S^3}\right) \tag{S10}$$

S2.4 Transition from in-plane yielding to wrinkling

Yield strength (MPa)	Stretch at which wrinkles appear
10	1.99
7.5	1.94
5	1.80
3.5	1.12[a]

[a] Wrinkles did not appear. The stretch of 1.12 corresponds to S_r when the net force in the sample is zero.

S2.5 Simulations of necking behavior

Fig. 10 in the main text shows a simulation with a plastic yield strength of 10 MPa subjected to stretching to a stretch of 2.86 and subsequent release. Fig. S6 shows the corresponding variation in film thickness at four different stretch values. Fig. S7 shows the simulated films with various values of the plastic yield strength. Both figures are discussed in detail in the text.

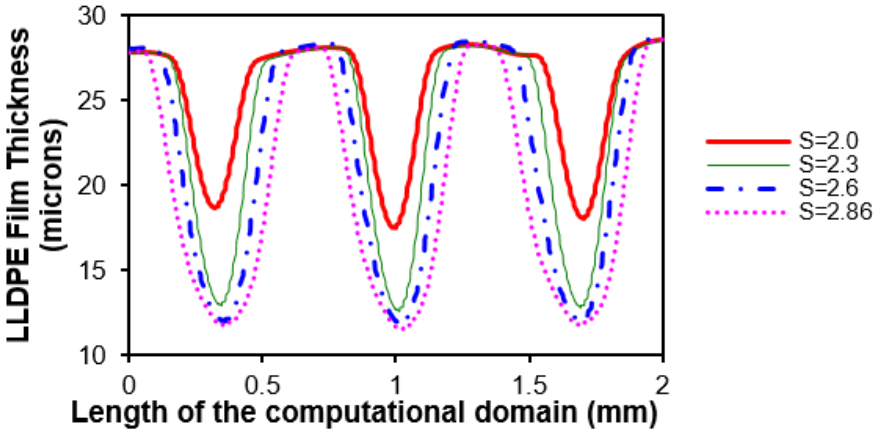

Fig. S6: Variation of plastic layer thickness along the length of the RVE at different stretch values.

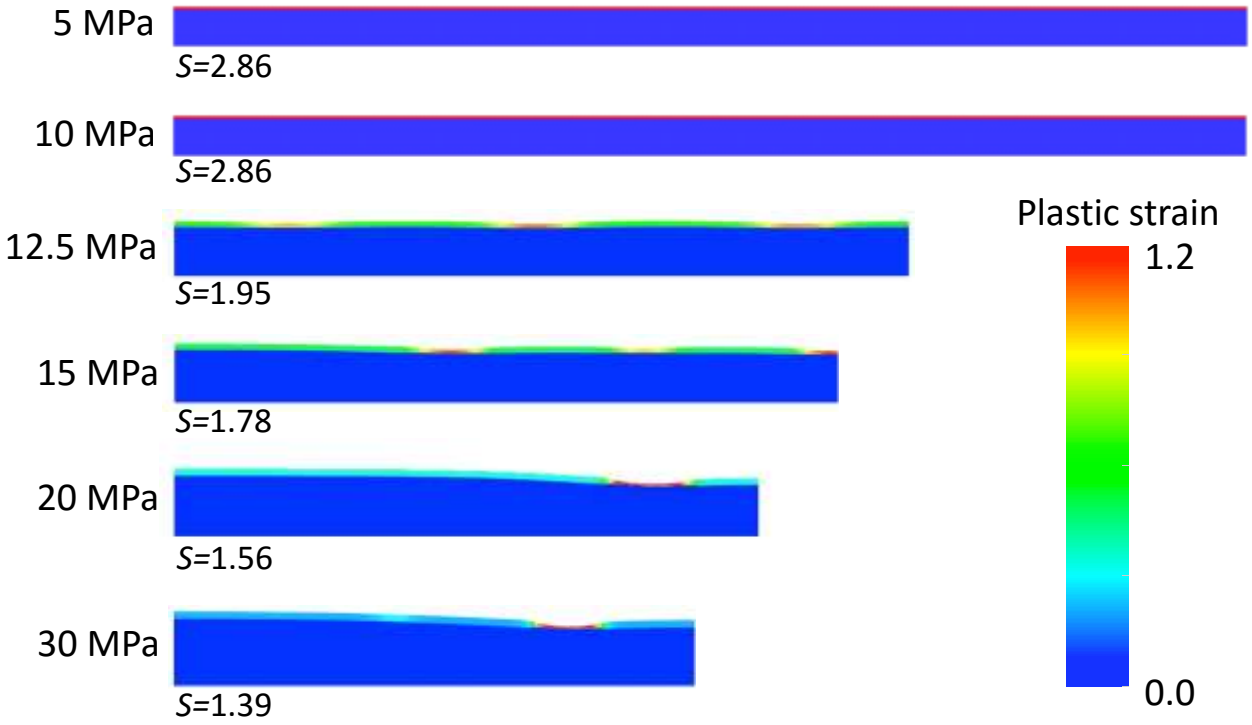

Fig. S7: Snapshots of stretching films at the various yield strengths listed. The stretch value of each snapshot is also listed.

S3 Elastic model

The physical picture is as follows: elastic films supported on softer elastic substrates wrinkle when some critical compressive stress is reached. When this critical stress is reached (at a stretch S_c) during release, wrinkles of wavelength λ_c appear everywhere on the film. Linear stability analysis of this situation under plane-strain conditions shows that[1]

$$\lambda_c = 2\pi h_{film}\left(\frac{\bar{E}_{film}}{\bar{E}_{substrate}}\right)^{\frac{1}{3}} \tag{S11}$$

where $\bar{E}_j = E_j/(1-\nu_j^2)$ is the modulus appropriate for plane strain conditions. In our experiments, h_{film} is 50 microns at the start of the experiment, but expected to change throughout the experiment. The value most relevant to the above equation is the film thickness h_c at the critical threshold for buckling. Since the free-standing plastic film does not undergo significant recovery, as a first approximation, the film dimensions are assumed to remain fixed during recovery. Thus, the film thickness during recovery can be taken to be

$$h_{film} = h_s = h_0 S_s^{-\frac{1}{2}} \tag{S12}$$

This equation assumes the kinematics of homogeneous uniaxial elongation. After buckling, as compression continues, the wavelength is expected to decrease geometrically in an accordion-like fashion to a final value:

$$\lambda_r = \lambda_c \frac{S_r}{S_c} \tag{S13}$$

Combining the above expressions yields

$$\lambda_r = 2\pi h_{film}\left(\frac{\bar{E}_{film}}{3\bar{E}_{substrate}}\right)^{\frac{1}{3}}\frac{S_r}{S_c} = 2\pi h_0 S_s^{-\frac{1}{2}}\left(\frac{\bar{E}_{film}}{3\bar{E}_{substrate}}\right)^{\frac{1}{3}}\frac{S_r}{S_c} \tag{S14}$$

We will now consider each of the quantities on the right hand side of Eq. S14 in turn. S_r is directly measured experimentally (Fig. 5b). S_c is more difficult to quantify since we were unable to measure the critical stretch at the wrinkling threshold. Specifically, the buckle amplitude and wavelength are both relatively small, and not visible with the visualization methods used in our experiments. Limited experiments were conducted on a custom stretching apparatus in our lab using a higher magnification camera which could be mounted much closer to the sample. Even in that case, the critical stretch was difficult to judge accurately. How then can S_c be estimated? We will follow the approach of Hu et al. [2] of using the stress-strain data to estimate S_c. This relies on the assumptions that the total force in the trilayer is a simple sum of the force in the rubber and the plastic, and that the load in the rubber layer in the trilayer is identical to the load in a free-standing rubber layer at the same nominal strain. Accordingly, we may estimate the load in the plastic layer at any nominal strain:

$$F_{plastic} = \frac{F_{trilayer} - F_{rubber}}{2} \tag{S15}$$

The factor of 2 in Eq. S15 simply accounts for the fact that there are two face layers. Fig. S8 shows the "raw data" of the $F_{trilayer}$ and F_{rubber} needed in Eq. S15, and the $F_{plastic}$ so-obtained is plotted in

Fig. S9A. It is interesting to note that the plastic contribution to the trilayer during the stretching is quite similar to the force of a free-standing plastic layer at the same nominal strain, i.e. coupling the plastic to the rubber (and hence suppressing necking) does not qualitatively change the stress-strain behavior of the plastic layer.

Regardless, during the release step, the calculated load in the plastic layer stays positive up to some value of nominal strain, beyond which it becomes negative. The point at which the load becomes zero may be regarded as the instant when the plastic first experiences compressive strain [2]. If we assume that the critical strain for wrinkling is quite small, then wrinkles must appear immediately after that point, i.e. the stretch at the zero load point may be regarded as nearly equal to S_c. The portion of the recovery step between S_c and S_r can then be regarded as compression beyond critical wrinkling. Fig. S9B&C plot S_c, S_r and their ratio S_r/S_c, which is relevant to Eq. S14.

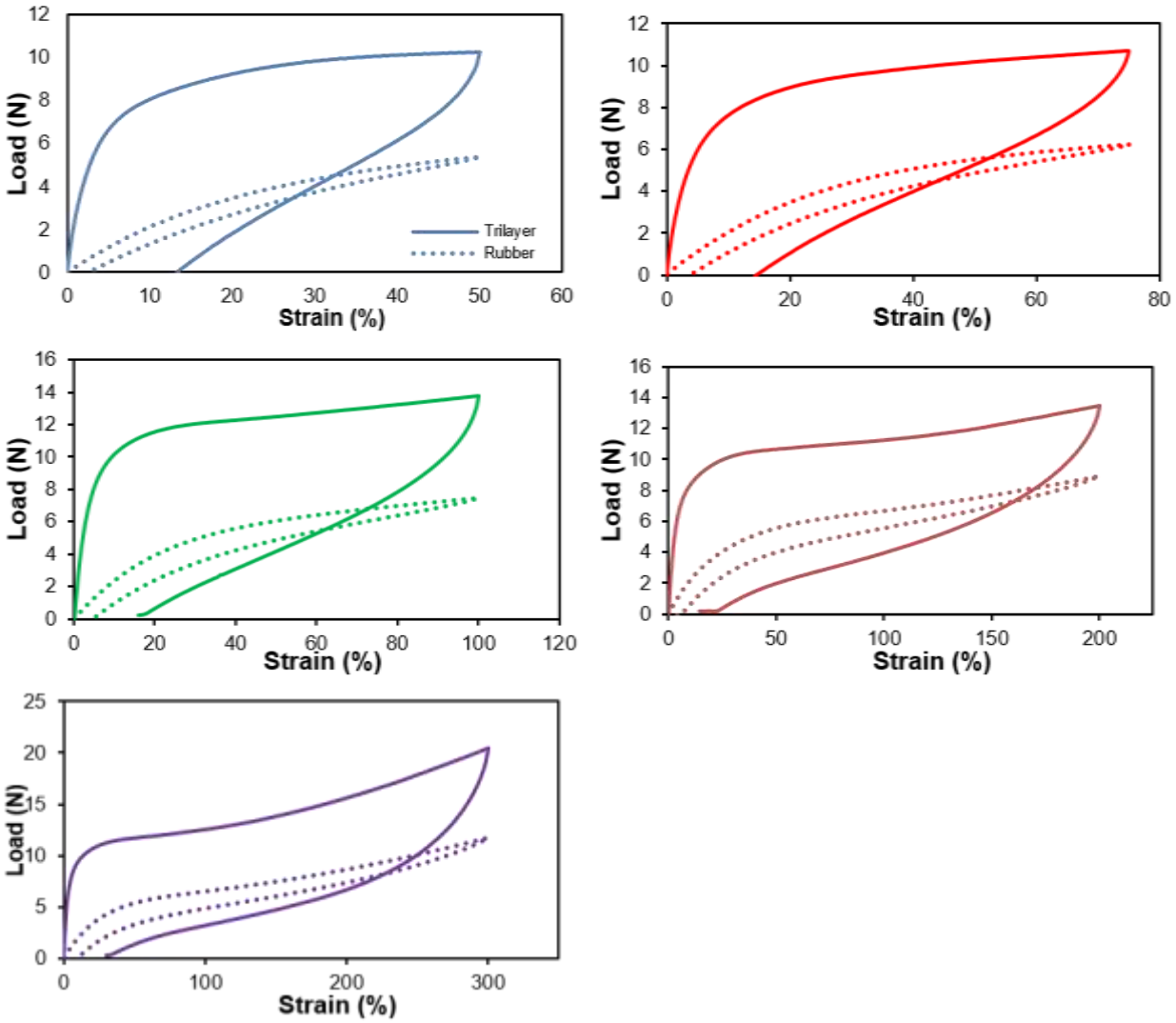

Fig. S8: Force vs nominal strain curves for the trilayer and the elastomer at various nominal strains. The difference between these curves corresponds to Fig. S9A below.

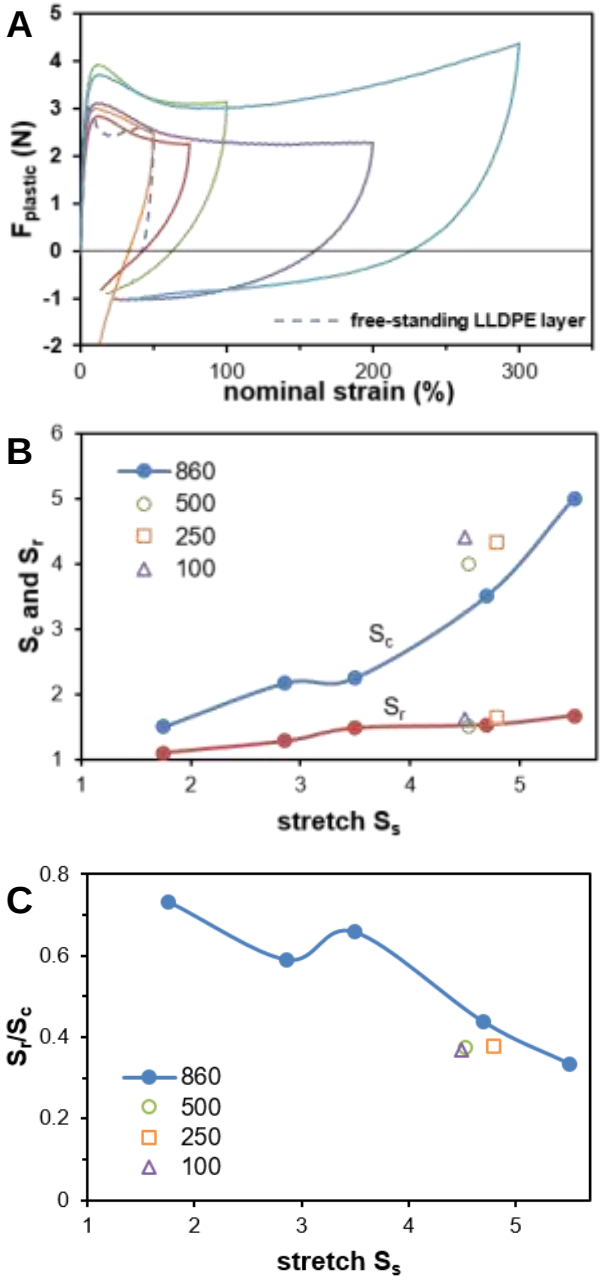

Fig. S9: (A) Load in the plastic layers calculated from Eq. S15. See Fig. S8 for the raw data used in subtraction. The dashed line corresponds to the same data as the LLDPE in Fig. 3D. (B) Stretch values S_c and S_r. The latter are the same data as in Fig. 5c. (C) Ratio S_r/S_c relevant to Eq. S14.

The last remaining quantity in Eq. S14 is the modulus ratio $\left(\frac{\bar{E}_{film}}{\bar{E}_{substrate}}\right)$. This is more difficult to estimate because what is relevant in Eq. S14 is not the ratio of the zero-strain modulus, but the ratio of the effective modulus in the neighborhood of the critical strain. Since the critical strain itself changes with S_s, the corresponding modulus must change as well. For the plastic layer, the problem is further compounded by the fact that the strain-strain relationship of the yielded plastic layer is difficult to measure directly; it may not be the same as that meausred during stretching and moreover, it may change with stretch. We have therefore used the modulus ratio as an adjustable parameter to compare Eq. S14 against the data. The solid line in Fig. S10 shows that reasonable agreement with the data is obtained if $\left(\frac{\bar{E}_{film}}{\bar{E}_{substrate}}\right)$ is taken to be 12 (any value between 10 and 16 gives comparable agreement). We must note however the modulus ratio of 12 used is much lower than the ratio (over 100) estimated from the small-strain region in Fig. 3D.

It is worth noting that Hu et al.[2] reported reasonable agreement between their model and experiments with no fitting parameters. However they ignored the fact that the plastic layer must become thinner due to stretching (i.e. they set $h_{film} = h_0$ instead of Eq. S12, a very poor approximation given that their nominal strains were as large as 600%). If they had accounted for the thinning of the plastic layer, their model would have been in poor agreement with their experiments.

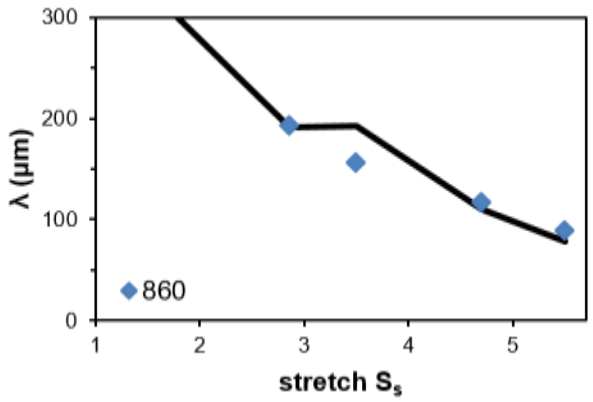

Fig. S10: Best fit of Eq. S14 to the measured wavelength data. The data are the same as from Fig. 6a from the main text.

References

1. Z. Y. Huang, W. Hong and Z. Suo, *Journal of the Mechanics and Physics of Solids*, 2005, **53**, 2101-2118.
2. Y. Hu, A. Hiltner and E. Baer, *Polymer Composites*, 2004, **25**, 653-661.